iR UNC Advantages and Real Geometrical Dimensions of Microband Electrodes

ARTICLE *in* ANALYTICAL CHEMISTRY · DECEMBER 1997

Impact Factor: 5.64 · DOI: 10.1021/ac970803d

5 AUTHORS, INCLUDING:

Ze'ev Porat
Nuclear Research Center - Negev
18 PUBLICATIONS **254** CITATIONS

SEE PROFILE

Anal. Chem. **1997,** *69,* 5073−5081

iR_{UNC} Advantages and Real Geometrical Dimensions of Microband Electrodes

Ze'ev Porat,[†] Joseph C. Crooker, Yining Zhang,[‡] Y. Le Mest,[§] and Royce W. Murray*

Kenan Laboratories of Chemistry, University of North Carolina, Chapel Hill, North Carolina 27599-3290

Microband electrodes have two important advantages relative to microdisks: (a) larger and thus more easily measured currents and (b) smaller ohmic drop (iR_{UNC}). Measurements of electrode kinetics and of transport under linear diffusion conditions at microband electrodes require knowledge of their actual areas. This paper describes the use of microbands, fabricated by sandwiching a thin metal film between insulators (sandwich electrode) and by lithographic deposition of a thin metal strip on an insulating substrate (line electrode), under radial and linear diffusion conditions, achieved using respectively fluid and highly viscous solutions. When compared under linear diffusion conditions to microdisk and line electrodes, most sandwich microband electrodes have actual areas that are larger than their planned, geometrical areas. The difference is not revealed under radial diffusion conditions. This paper also describes linear diffusion experiments which test the theory that predicts smaller iR_{UNC} effects at microbands relative to those at microdisks.

This research was initiated[1] in support of a project on solid state voltammetry based on using polyether polymer electrolytes[2] as model solids and semisolids. The small diffusion coefficients (D) of redox solutes in these media, and their typically low ionic conductivities, require voltammetric tools that yield measurable currents yet do not develop devasting uncompensated resistances (R_{UNC}). Microdisk electrodes have many attractive properties,[3] but microdisk currents can be sufficiently small as to be difficult to measure. For example, the limiting current for a 1 mM electron donor solution in which $D = 10^{-12}$ cm^2/s (a "moderately" small value in a semisolid) would be only 0.2 fA at a 5 μm radius (r) microdisk electrode.

Our laboratory has approached semisolid phase measurements[2] by using hybrid redox polyethers that are highly concentrated in redox centers (0.1−1 M),[2c−f,h,i] by careful instrument design, and (where needed) with microband electrodes. Microbands are attractive because microelectrode theory predicts both larger currents and improved uncompensated resistance properties (or at least not degraded ones) relative to those of microdisks. Attaining such pleasing but seemingly contradictory properties has, however, not been previously verified by experimental tests, and examining these aspects of microband electrode theory was one purpose of the present investigation.

Another purpose of the investigation was to use linear diffusion conditions to experimentally evaluate the *real* areas of several fabricated versions of sandwich-type (exposed edge of metal film sandwiched between insulating phases) microbands. Linear diffusion conditions prevail in fluid solutions on short electrolysis time scales,[4] but in viscous media, like the polyethers, diffusion can be linear even on long time scales. (For reference, while a typical fluid solution diffusion coefficient is 10^{-5} cm^2/s, we have encountered[5] values as small as 10^{-18} cm^2/s in polyether media.) In linear diffusion geometry, the observed currents depend on the surface area of the electrode available to a diffusing solution species, or, more exactly, on the surface area that is determined by microscopic features comparable in size to the diffusion layer depth. A diffusion layer depth can be molecule-sized,[2c] so linear diffusion can provide a highly sensitive probe of whether a microband electrode's real working area differs from that of its nominal area. In fact, we find very substantial deviations from nominal microband areas that tests using radial diffusion results *do not reveal*.

Evaluation of real microband areas using linear diffusion currents, of course, requires knowledge of the diffusion coefficients of the electroactive species in the electrolyte media employed. The D values were determined using microdisk electrodes (in some cases of nominal area equal to that of the microband) and, in a few cases, with lithographically fabricated line electrodes, implicitly assuming those electrodes to have actual areas equal to their nominal values. Failure of the latter assumption means that the real microband areas are even larger than reported, but we regard the assumption as reasonably secure, since microdisk and lithographic line electrode values for D agree (where used on the same redox system).

[†] Permanent address: Department of Analytical Chemistry, Nuclear Research Center−Negev, P.O. Box 9001, Be'er Sheva, Israel.

[‡] Permanent address: Kemet Electronics Corp., 201 Fairview St. Ext., P.O. Box 849, Fountain Inn, SC 26844.

[§] Permanent address: University Bretagne Occidentale, URA CNRS 322, Lab. Chim. Electrochim., & Chim. Analyt., BP 809, F-29285 Brest, France.

(1) Le Mest, Y., The University of North Carolina at Chapel Hill, unpublished results, 1989.

(2) (a) Longmire, M. L.; Watanabe, M.; Zhang, H.; Wooster, T. T.; Murray, R. W. *Anal. Chem.* **1990**, *62*, 747. (b) Wooster, T. T.; Longmire, M. L.; Zhang, H.; Watanabe, M.; Murray, R. W. *Anal. Chem.* **1992**, *64*, 1132. (c) Poupart, M. W.; Velazquez, C. S.; Hassett, K.; Porat, Z.; Haas, O.; Terrill, R. H.; Murray, R. W. *J. Am. Chem Soc.* **1994**, *116*, 1165. (d) Haas, O.; Velazquez, C. S.; Porat, Z.; Murray, R. W. *J. Phys. Chem.* **1995**, *99*, 15279. (e) Terrill, R. H.; Hatazawa, T.; Murray, R. W. *J. Phys. Chem.* **1995**, *99*, 16676. (f) Velazquez, C. S.; Murray, R. W. *J. Electroanal. Chem.* **1995**, *396*, 349. (g) Pyati, R.; Murray, R. W. *J. Electrochem. Soc.* **1996**, *143*, 401. (h) Long, J.; Velazquez, C. S.; Murray, R. W. *J. Phys. Chem.* **1996**, *100*, 5492. (i) Williams, M. E.; Masui, H.; Long, J. W.; Malik, J.; Murray, R. W. *J. Am. Chem Soc.* **1997**, *119*, 1997.

(3) Wightman, R. M.; Wipf, D. O. *Electroanalytical Chemistry*; Vol. 15. Bard, A. J., Ed.; M. Dekker, Inc.: New York, 1989.

(4) Wightman, R. M. *Science* **1988**, *240*, 415.

(5) Crooker, J. C., The University of North Carolina at Chapel Hill, unpublished results, 1996.

S0003-2700(97)00803-2 CCC: $14.00

In principle, electron transfer kinetics, double-layer charging capacitance, and underpotential metal deposition/stripping are also specific surface area-dependent phenomena that could be exploited to assess actual microelectrode areas. Capacitance has, indeed, been previously used to examine the quality of metal/insulator seals.[6] Compton et al.[7] have engaged in theoretical simulations of various geometrical nonidealities of microband electrodes.

The investigation of linear diffusion-based microband areas will be presented in the first part of the paper and microband iR_{UNC} properties in the second.

EXPERIMENTAL SECTION

Equipment. Locally built, low-current potentiostats[8] were employed inside Faraday cages, one controlled by a universal programmer (EG&G PAR Model 175) and the other by a PC using a locally written program. Gold films were deposited using a metal evaporator (Model KV-301, Key High Vacuum) and their thicknesses measured with a step profilometer (Tencor Alfa-step 100) having a resolution of 50 Å. Optical microscopy was carried out using a Zeiss universal microscope and scanning electron microscopy (SEM) with a Phillips Model 505 operated at an acceleration voltage of 30 kV.

Materials. Tefzel film samples were supplied by DuPont-Higher Performance Films Division. Gold-coated glass and alumina slides were purchased from Evaporated Metal Films Inc. (Ithaca, NY) and Materials Research Corp. (Orangeburg, NY), respectively. Acetonitrile and monomethyl polyethyleneoxide (MW 400, MePEG-400) were distilled and stored over molecular sieves. Tetraethylammonium perchlorate (Et_4NClO_4), ferrocenecarboxylic acid ($CpFeCpCO_2H$), and ferroceneethanol ($CpFeCpCH_2CH_2OH$) (Aldrich) were recrystallized. Lithium perchlorate was dried overnight at 120 °C and stored in an inert atmosphere glovebox. Other chemicals were analytical grade and used as received.

Microband Fabrication. The methods used are summarized here. A more detailed description for types A, B, and D can be found in the Supporting Information. The electrode designations follow Table 1.

Type A. Commercial 0.65 cm × 10 cm gold-coated (both sides) alumina wafers (Al_2O_3/500 Å Cr/ 300 nm Au, Materials Research Corp.) were cut to 0.65 cm × 1.0 cm squares and sandwiched between glass slides using Tefzel films (a heat-bondable Teflon, 20−30 min at 300−320 °C) as sealant. One end was polished to expose two nominally 300 nm wide microbands, which could be used as independent microband specimens. Types A1 and A2 were prepared as type A but respectively using epoxy as sealant or depositing a 500 nm layer of Si_3N_4 on the Au faces, followed by epoxy sealant (curing the Epon epoxy sealant at 65 °C overnight).

Type B microbands were fabricated by covering both sides of a thin evaporated Au film with wet epoxy, as follows: A Au film was evaporated onto a glass slide that had been silanized with a hydrophobic reagent so as to give poor adhesion and then covered with a layer of wet epoxy that was then cured. It was next separated from the glass slide to give an epoxy-supported Au film, which was then covered with wet epoxy and cured. Microbands (nominally from 130 nm to 6 μm wide and 0.70 cm long) were exposed by polishing or microtoming. Type B1 microbands were fabricated by evaporating a 286 nm gold film onto a cured epoxy flat, followed by covering the gold film with a second layer of wet epoxy, curing it. Microbands on the working edge of the resulting 0.7 cm long electrodes were exposed either by polishing or by microtoming. The aim of type B and B1 procedures was to form a working electrode surface surrounded by thick layers of insulating materials of equal hardness, seeking to avoid differential stress during polishing. The nominal surface area (2×10^{-5} cm^2) of a 286 nm thick, 0.7 mm long Au microband was equal to that of a 25 μm radius microdisk.

Table 1. Results and Predictions for Radial and Linear Diffusion-Controlled Microband Currents

electrode type	w, μm	L, cm	I_{rad}, nA exptl	I_{rad}, nA theor[a]	lin diffus, CV[b] $[I_{P,band}/A]/[I_{P,disk}/A]$	lin diffus, CA[c] $[S_{band}/A]/[S_{disk}/A]$
A	0.300	0.65	581 ± 74[d]	558[d]	3.3[e]	
A	0.300	0.65	412 ± 20[f]	420[f]	10 ± 6[g]	
A1	0.300	0.65	397 ± 18[f]	420[f]	13 ± 5[g]	
A2	0.200	1.0	578 ± 7[f]	600[f]	13 ± 3[g]	
B	0.136	0.7	447[d]	535[d]		
B1	0.286	0.7	380[f]	405[f]	∼100[g]	
C	28	0.3	490[f]	487[f]	0.96[n]	
C	28	0.35	555 ± 5[f]	569[f]	1.0[o]	
D	2.7	0.7	95[h]	87[h]	1.0,[i] 1.4[j]	
D-old	2.7	0.7				19[k]
D-old	2.7	0.7				12.6 (±1.9)[l]
line	10	0.2				1.05[m]

[a] Calculated from eq 5. Expts are averages of 2−10 experiments. [b] Comparison of (nominal) area-normalized cyclic voltammetric peak currents at microbands and microdisks under conditions where i_p is proportional to the square root of potential scan rate. [c] Comparison of (nominal) area-normalized slopes of Cottrell plots (chronoamperometric potential step experiments) obtained at microbands and microdisks under conditions giving linear current vs $t^{-1/2}$ plots with near-zero intercepts. [d] 1 mM $CpFeCpCH_2CH_2OH$ in 0.1 M Et_4NClO_4/CH_3CN, $D = 1.8 \times 10^{-5}$ cm^2/s, $\nu = 0.1$ V/s. [e] 10 mM $[CpFeCpCH_2N(CH_3)_3^+][PF_6^-]$ in 0.1 M $LiClO_4$/MePEG-400, −17 °C, $\nu = 10$ V/s, microband compared to 25 μm radius Pt microdisk; $A_{band} = A_{disk}$; $D = 2.2 \times 10^{-8}$ cm^2/s. [f] 1 mM $CpFeCpCO_2H$ in 0.1 M Et_4NClO_4/CH_3CN, $D = 1.55 \times 10^{-5}$ cm^2/s , $\nu = 0.01$ V/s. [g] Varied results in polyether media, depends on specific electrode sample, redox couple/polyether solvent combination, history of polishing, and previous solvent exposure. [h] 10 mM $CpFeCpCO_2H$ in "wet" 1.5 M $LiClO_4$/MePEG-400, 25 °C, 2 mV/s, $D = 1.7 \times 10^{-7}$ cm^2/s as measured with a microdisk electrode. [i] 1 mM $CpFeCpCH_2CH_2OH$ in 0.1 M $LiClO_4$/glycerol, −11 °C, nominal area of microband is 10× that of 24 μm radius microdisk, $D = 5 \times 10^{-10}$ cm^2/s. [j] Same as *i* but at 1 °C ($D = 1.3 \times 10^{-9}$ cm^2/s), with a different type D electrode. [k] Microband like preceeding type D entries, except after 3 years of intermittent use; chronoamperometry in an undiluted melt of $[Co(bpy(CO_2\text{-MePEG-350})_2)_3](ClO_4)_2$, $D = 5 \times 10^{-12}$ cm^2/s. The nominal area-normalized Cottrell plot slopes from microband experiments (S_{band}/A) are compared to the average of area-normalized Cottrell slopes (S_{disk}/A, 5.2×10^{-5} and 5.2×10^{-5} (A sec$^{1/2}$)/cm^2) from experiments in the same melt with 95 and 57 μm radius Pt microdisks, respectively. [l] Microband like *k*, also after 3 years of intermittent use, chronoamperometry in an undiluted melt of $[Co(bpy(CO_2PPPM)_2)_3](ClO_4)_2$ (with ∼5% excess Co salt), $D = 2 \times 10^{-14}$ cm^2/s. The average 12.6-fold real-area factor was determined by comparing nominal area-normalized Cottrell plot slopes (S_{band}/A) from four microband determinations to the average of area-normalized Cottrell slopes (S_{disk}/A, 3.9×10^{-6} and 4.2×10^{-6} (A sec$^{1/2}$)/cm^2) from experiments in the same melt with a 6.5 μm radius Pt microdisk and a 10 μm wide, 0.2 cm long, lithographically-defined Pt line electrode, respectively. Figure 7 shows these data, with the 12.6 real-area factor included in the area-normalized current axis. [m] Lithographically prepared Pt line electrode, average slopes from Cottrell plots from chronoamperometry as in Figure 7, compared to 6.5 μm radius Pt microdisk electrode, in $[Co(bpy(CO_2PPPM)_2)_3](ClO_4)_2$ (which by analysis contained ∼5% excess Co salt); $D = 1.6 \times 10^{-14}$ cm^2/s. [n] 10 mM $[CpFeCpCH_2N(CH_3)_3^+][PF_6^-]$ in 0.1 M $LiClO_4$/MePEG-400, $\nu = 10$ V/s, microband compared to 25 μm radius Pt microdisk; $A_{band} = 42.8A_{disk}$. [o] Same as *n* but $A_{band} = 50A_{disk}$.

(6) Wehmeyer, K. R.; Wightman, R. M. *J. Electroanal. Chem.* **1985**, *196*, 417.
(7) (a) Alden, J. A.; Booth, J.; Compton, R. G.; Dryfe, R. A. W.; Sanders, G. H. W. *J. Electroanal. Chem.* **1995**, *389*, 45. (b) Alden, J. A.; Compton, R. G. *Electroanalysis* **1996**, *8*, 30.
(8) Woodward, S. W., design consultant, The University of North Carolina at Chapel Hill.

Type C microbands were much wider, being fashioned from commercial 28 μm Pt foil sandwiched between glass slides with Tefzel films as sealant (as in type A). A Ag wire reference electrode was placed near the end of the Pt foil, and a 26 gauge Pt wire was placed near its side as a counter electrode.

Type D microbands were 0.7 cm long and included nearby, flanking reference and counter electrodes. Commercial Pt microfoils (nominal 2 μm, but actually 2.7 μm thickness as measured with an optical microscope) were separated by 2 μm thick Mylar films from two flanking 25 μm wide Ag microband reference electrodes, themselves flanked by the ends of two Pt rod counter electrodes. The Pt microfoil and flanking Ag foils and Pt rod counter electrodes were potted in an epoxy rod, the end of which was polished to expose the electrode assembly. The type D electrode with nearby Ag reference electrodes was fabricated expressly for use in semisolid, highly viscous polyether polymer electrolytes, to minimize uncompensated resistance effects. Additional reference electrodes (far-away reference) were placed ~3 mm away from the Pt microband to study the influence of distance on the uncompensated solution resistance.

Microdisk. A Pt microdisk with a nearby reference electrode was prepared by placing a drop of freshly mixed epoxy and then a silver foil (~1 cm long, 5 mm wide, and 25 μm thick) on a pad of hardened Epon epoxy, followed by another drop of fresh epoxy, and then a 2 μm thick Mylar film, followed by a third drop of fresh epoxy, a ~100 μm diameter Pt wire, and another pad of hardened epoxy. This "sandwich" was clamped and cured (2 h at 80 °C, then 2 h at 150 °C), leads were attached, and the sandwich was embedded in epoxy using a Teflon tube mold, followed by sanding and polishing to expose the electrodes.

RESULTS AND DISCUSSION

Theory for Microband Currents. Microelectrode diffusion geometry can be characterized by the dimensionless parameter ϕ,

$$\phi = \left(\frac{\sqrt{Dt}}{r}\right)^2 \tag{1}$$

where D is diffusion coefficient, t is time, and r is the smallest dimension of the electrode.[3] When $\phi \ll 1$ (small t and/or small D and/or large r), linear diffusion geometry prevails, and a linear potential sweep and a reversible electrode reaction give a current–potential curve with peak current expressed by the Randles–Sevcik equation (at 25 °C):

$$i_p = (2.69 \times 10^5) n^{3/2} A v^{1/2} D^{1/2} C \tag{2}$$

where A is electrode area and v is potential sweep rate. Equation 2 applies to both microdisk and microband, with $A = \pi r^2$ for a microdisk and $A = wL$ for a microband, where w is width and L length.

For ϕ near unity, the diffusion geometry is a mix of linear and radial diffusion. Exact analysis of the peak-shaped current–potential curve resulting from a potential sweep is more complex, but relations are available, such as that for a microband by Aoki:[9]

$$i_p = nFCDL\left[0.439p + 0.713p^{0.108} + \frac{0.614p}{1 + 10.9p^2}\right] \tag{3}$$

$$\text{where} \qquad p = \left(\frac{nFw^2v}{RTD}\right)^{1/2}$$

When $\phi \gg 1$, radial diffusion becomes predominant, and the potential sweep voltammogram loses its peak shape and displays plateaued current–potential curves that are only slightly dependent on (microband) or completely independent of (microdisk) the potential sweep rate. The equations depend on the microelectrode shape, and for a microdisk the limiting current is[3,10]

$$i_{LIM} = 4nFrDC \tag{4}$$

For a microband, the radial diffusion chronoamperometric (potential step) expression for a hemicylinder of radius r gives the current response on a microband of equivalent area, if r is substituted[10b,11] by $w/4$. This equation gives the current for a potential sweep experiment by substituting $t = RT/nFv$. These two relations are, serially,

$$i = \frac{\pi nFDCL}{\ln[8\sqrt{Dt}/w]} = \frac{\pi nFDCL}{\ln[1.28\sqrt{D/v}/w]} \tag{5}$$

Equation 5 shows the following: (a) The microband currents are not truly steady state but decay only gradually with time. (b) Microdisk radial diffusion currents are proportional to disk radius (eq 4), while for the microband, current is proportional to microelectrode length L and is relatively *insensitive* to the microband width. For example, two microbands of equal L but with w differing by 10^3-fold (1 μm and 1 nm) give limiting currents differing only by a factor of 7. (c) For microdisks and microbands of equal area, linear diffusion currents (eq 2) are the same, but radial currents are much larger at the microband. The latter comes about because the microband has a larger ratio of perimeter to surface area and thus a larger edge diffusion flux.

Additionally, for microbands nearing molecular dimensions (w < 20 nm), it has been reported[12] that observed currents are lower than those predicted by eq 5, i.e., for *very* small electrodes, additional phenomena have to be incorporated into the transport theory.

Figure 1 illustrates an imperfect microband with a crack caused by delamination (or cracking) of the metal–insulator seal. At the top, in an experiment where $\phi > 1$ (radial diffusion), the observed currents will be near steady state as soon as the volume of solution contained within the crack is exhausted of its electroactive species. The observed radial current is determined primarily by the horizontal part of the microband exposed to the solution and can exhibit a nearly ideal value, i.e., diffusionally, the crack disappears. On the other hand, at the bottom of Figure 1, where $\phi \ll 1$ (linear diffusion), the electrode surface area to which linear diffusion

(9) Aoki, K. *Electroanalysis* **1993**, *5*, 627.

(10) (a) Saito, Y. *Rev. Polarogr. Jpn.* **1968**, *15*, 177. (b) Kovach, P. M.; Caudill, W. L.; Peters, D. G.; Wightman, R. M. *J. Electroanal. Chem.* **1985**, *185*, 285.

(11) Amatore, C. A.; Fosset, B.; Deakin, M. R.; Wightman, R. W. *J. Electroanal. Chem.* **1987**, *225*, 33.

(12) (a) Wehmeyer, K. R.; Deakin, M. R.; Wightman, R. M. *Anal. Chem.* **1985**, *57*, 1913. (b) Morris, R. B.; Franta, D. J.; White, H. S. *J. Phys. Chem.* **1987**, *91*, 3559.

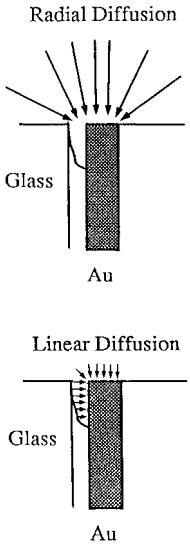

Figure 1. Cartoon of microband with delamination defect, illustrating influences on linear and radial currents.

occurs is the sum of the vertical and horizontal sections of the electrode. Clearly, a 1 μm deep delamination of a 100 nm wide band can cause a *major* change in the observed linear diffusion currents.

Previous Microband Fabrications. Microband electrodes are of two major designs: (i) the exposed edges of metal films (microfoil or evaporated/sputtered films) sealed between two insulators (e.g., glass, epoxy, etc.) and (ii) photolithographically deposited thin, narrow strips (lines) of metal on an insulating plane.

A variety of "sandwich-type" bands have been reported. Wightman and co-workers[3,4,13] melted a slotted glass tube around a Pt microfoil and epoxied Pt or Au microfoils between metal film-coated glass slides to blank glass slides. Bond et al.[14] used gold films evaporated on glass plates and polyester sheets, again sealed with epoxy to another glass slide. Paired microbands were constructed by Hill et al.[15] by epoxying two gold-coated glass slides together with a Teflon spacer, and by Shea and Bard[16] from thin mica sheets with sputtered Pt on both sides, sandwiched between glass slides with epoxy. Analogous procedures but different materials were used by Zadeii et al.,[17] Wang et al.[18] (for microbands), and Odell and Bowyer[19] (for a microband array). Morris et al.[12b] embedded ultrathin Au and Pt films on cleaved mica sheets in epoxy blocks.

Sandwich-type microbands have generally (with interesting exceptions[12]) performed in accordance with radial diffusion theory. Effects of the finishing of the microband surface on the radial theoretical performance have also been considered, for example, by Shea and Bard,[16] with observed currents and waveshapes substantially unchanged. In most reports, the final surface finishing includes fine polishing (e.g., 0.05 μm alumina).

Sandwich-type microbands, including those prepared in this paper, are subject to delamination defects, as illustrated in Figure 1. By examining a variety of fabrication procedures, the present results (vide infra) indicate that such defects are a general problem. (Many practicing electrochemists probably already appreciate this, but it has not been previously reported in depth, nor by use of slow diffusion media.) Except for type D microbands, none of the fabrication procedures is especially distinctive from those reported in the previous literature.

Photolithography has also been employed to fabricate microbands[20−22] and their cousins, interdigitated array electrodes.[23] Lithographic fabrication produces metal (Au, Pt) or carbon strips (lines) resting atop an insulator (glass, SiO_2-on-Si). The line microband width (1−20 μm) greatly exceeds its height (typically 100−200 nm). Lithography can access any desired configuration of microband length, width (except submicrometer), and interdigitation but requires a special facility for production. Another advantage is freedom from defects like that in Figure 1. An analogous delamination defect could, in principle occur by undercutting, but the actual area change would be 2-fold at most and, in practice, the conducting line would fracture and lose electrical contact before such a large change could occur. For this reason, we regard line microbands and microdisks as more reliable "standards" and employ them to evaluate diffusion coefficients in linear diffusion conditions.

Evaluation of Microband Currents. Results for radially and linearly diffusion-controlled currents at the variously fabricated microbands are given in Table 1 and will be discussed serially as listed. Specific details regarding the media employed are found in the Table 1 footnotes.

Figure 2 gives examples of voltammograms observed (CpFeCpCH$_2$CH$_2$OH in CH_3CN solution) at type A (w = 300 nm) electrodes under radial diffusion conditions. Of 23 electrodes fabricated, 10 showed voltammograms with similar limiting currents (i.e., curves A−C). Curve A is a nearly ideal radial diffusion example. The tilted curve B suggests a serial ohmic resistance such as a polishing process residue; cleaning the surface with acetone and rubbing with a soft cloth often eliminated this effect. Other examples (curve D) gave significantly smaller currents and could not be rejuvenated. Substantial capacitance currents in some examples (curve C) suggest larger real surface areas. Nonetheless, the limiting currents in Figure 2, curves A−C, and those observed using a different ferrocene reactant (CpFeCpCO$_2$H), and with type A1 and A2 microbands, are close to those predicted (Table 1, electrodes A, A1, and A2, experimental vs theoretical I_{rad}) from radial diffusion theory (eq 5) using D values measured with microdisk electrodes in the same solutions. Although the 40% fabrication success rate of type A electrodes requires an evaluation step, the simple procedure and commercial availability of its components are attractive where radial diffusion conditions are expected.

In fluid solvents such as CH_3CN, the narrow (w = 200−300 nm) type A electrodes would require microsecond time scales to

(13) Deakin, M. R.; Wightman, R. M.; Amatore, C. A. *J. Electroanal. Chem.* **1986**, *215*, 49.
(14) Bond, A. M.; Henderson, T. L. E.; Thormann, W. *J. Phys. Chem.* **1986**, *90*, 2911.
(15) Hill, H. L. O.; Klein, N. A.; Psalti, I. S. M.; Walton, N. J. *Anal. Chem.* **1989**, *61*, 2200.
(16) Shea, T. V.; Bard, A. J. *Anal. Chem.* **1987**, *59*, 2101.
(17) Zadeii, J. M.; Mitchell, R.; Kuwana, T. *Electroanalysis* **1990**, *2*, 209.
(18) Wang, J.; Brennsteiner, A.; Sylwester, A. P.; Renschler, C. L. *Electroanalysis* **1991**, *3*, 505.
(19) Odell, D. M.; Bowyer, W. J. *Anal. Chem.* **1990**, *62*, 1619.
(20) Samuelsson, M.; Armgarth, M.; Nylander, C. *Anal. Chem.* **1991**, *63*, 931.
(21) Morita, M.; Longmire, M. L.; Murray, R. W. *Anal. Chem.* **1988**, *60*, 2770.
(22) Kittlesen, G. P.; White, H. S.; Wrighton, M. S. *J. Am. Chem. Soc.* **1984**, *106*, 7389.
(23) (a) Chidsey, C. E. D.; Feldman, B. J.; Lundgren, C.; Murray, R. W. *Anal. Chem.* **1986**, *58*, 601. (b) Takahashi, M.; Morita, M.; Niwa, O.; Tabei, H. *J. Electroanal. Chem.* **1992**, *335*, 253. (c) Niwa, O.; Morita, M.; Tabei, H. *Electroanalysis* **1994**, *6*, 237. (d) Niwa, O.; Xu, Y.; Halsall, H. B.; Heineman, W. R. *Anal. Chem.* **1993**, *65*, 1559.

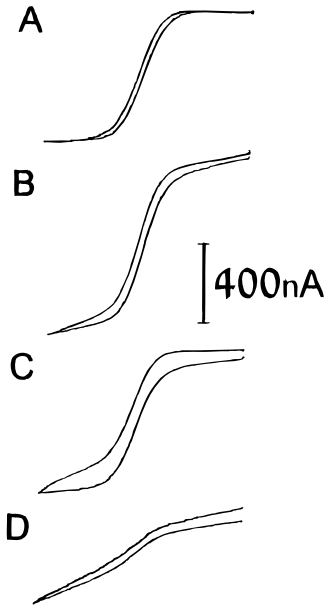

Figure 2. Examples of radial diffusion voltammograms at type A microbands; 1 mM $CpFeCpCH_2CH_2OH$ in 0.1 M Et_4NClO_4/CH_3CN.

achieve linear diffusion conditions ($\phi < 1$). Alternatively, viscous media, wherein the electroactive substances diffuse slowly, can be employed, as in Figure 3 (top), where a type A microband and a 25 μm radius microdisk (has the same nominal area) are compared in a polyether electrolyte at reduced temperature and modest potential scan rates. The microband example (curve A, top) has a resistive tilt, but the peak current is easily measured. Linear diffusion conditions are attained at both electrodes, as demonstrated in Figure 3 (bottom), which shows accord with eq 2. The Figure 3 (bottom) comparison shows clearly that the microband currents are larger than expected relative to the microdisk; i.e., the real microband area is larger than its nominal value by about 3-fold (Table 1, lin diffus, CV). Other tests with types A, A1, and A2 electrodes in a variety of polyether media (Table 1) revealed even larger (>10-fold) real microband areas. The excess microband areas may arise from cavities or delamination along the insulator−gold interface (Figure 1); we were unsuccessful, however, in imaging these defects using SEM. Whatever the details of origin, the real microband areas are clearly larger than nominal, a fact not revealed under radial diffusion conditions.

Types B and B1 fabrication provides macroscopic sections of the same insulator on both sides of the Au film. In fluid solvents, these electrodes gave an assortment of responses like those in Figure 2, and like type A electrodes, their radial diffusion currents were near those predicted (Table 1). However, most samples exhibited serial resistances like Figure 2B, were sensitive to electrode history (prior use at lowered temperature or in organic solvents), and, in spite of detailed variations in fabrication and polishing, displayed very poor performance (larger currents than nominal) under linear diffusion conditions (polyether media, reduced temperatures). The excess microband area (relative to microdisk area) was as large as ~100-fold and highly variable from example to example. Delamination is evident in the Figure 4A micrograph of a type B electrode, clearly showing a large gap between epoxy insulator and Au and "smoking gun" evidence for the origin of excess real microband areas.

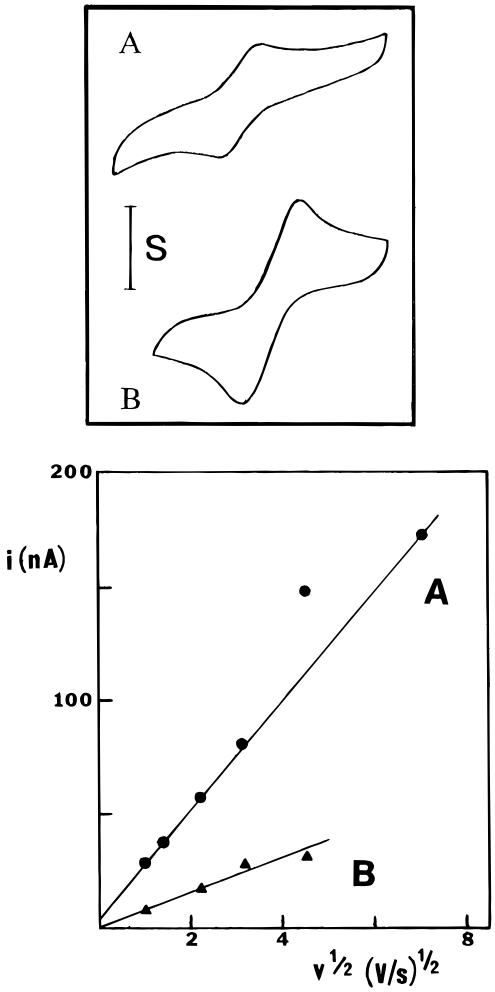

Figure 3. Cyclic voltammograms (10 V/s) (top) and plots of i_p vs $v^{1/2}$ (bottom) of 10 mM $CpFeCpCH_2N(CH_3)_3^+$ in 0.1 M $LiClO_4$/MePEG-400 at −17 °C, at a type A microband (curve A, $S = 200$ nA) and a microdisk of identical nominal area (curve B, $S = 25$ nA).

We do not claim it impossible to use thin, evaporated metal films in sandwich-type microbands to produce electrodes with equal real and nominal areas. However, the above linear diffusion real area determinations serve to demonstrate that microband electrodes can possess substantial excess area yet produce radial diffusion currents reasonably close to theory. Wehmeyer et al.[12a] also detected imperfections in very thin sandwich-type microbands based on 30−100-fold discrepancies in background (charging) currents, relative to larger electrodes. It is appropriate to note, however, that our linear diffusion results obtained are in the opposite direction to account for the interesting results of Morris et al.[12b]

We turn next to sandwich-type microbands made from thick metal microfoils. A micrograph top view of a 2.7 μm wide type D microband is shown in Figure 4B. The spacing produced by the Mylar films and epoxy sealant between the Pt microfoil and nearby Ag reference electrodes is about 3 μm, very close to the nominal microband width. The far-away Ag reference electrodes of this assembly are not seen in the micrograph.

Type D microbands typically gave very well-behaved radial diffusion voltammetry, as exemplified by the room temperature, slow potential sweep experiment in a "wet" polyether solvent in Figure 5A ($D = 1.7 \times 10^{-7}$ cm^2/s). The plateau current is reasonably close to the predicted radial diffusion value (Table 1).

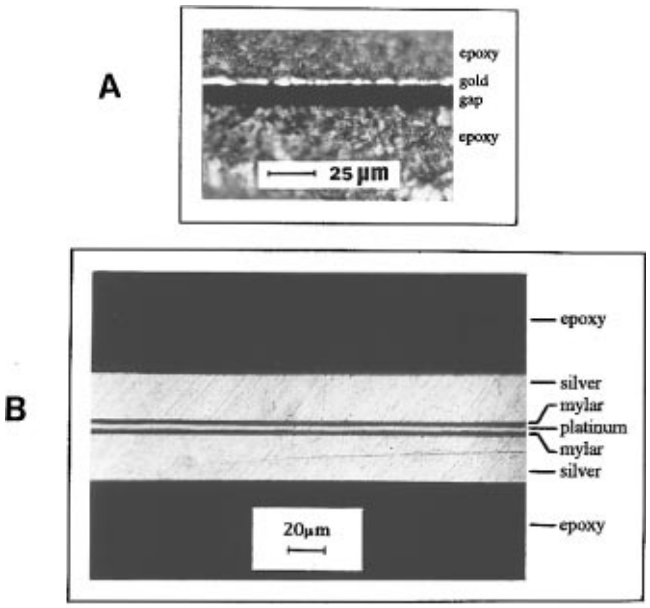

Figure 4. (A) Optical micrograph of a type B microband, showing delamination between the first layer of epoxy and the evaporated gold film. (B) Optical micrograph of a type D Pt microband ($w = 2.7$ μm) with two nearby Ag reference electrodes.

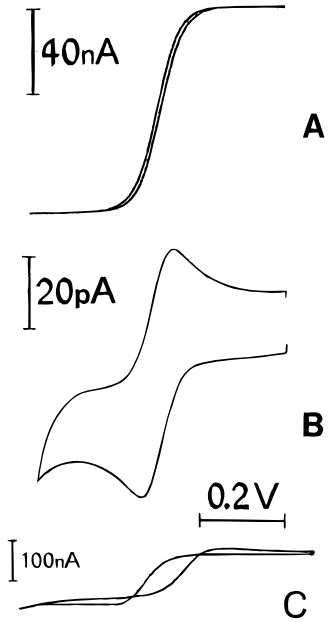

Figure 5. Cyclic voltammograms recorded with type D ($w = 2.7$ μm) Pt microband. Curve A: radial diffusion of 10 mM $CpFeCpCO_2H$ in "wet" 1.5 M $LiClO_4$/MePEG-400, 25 °C, $v = 2$ mV/s, far-away Ag reference. Curve B: linear diffusion of 1 mM $CpFeCpCH_2CH_2OH$ in 0.05 M $LiClO_4$/glycerol, −11 °C, $v = 1$ mV/s, nearby Ag reference. Curve C: radial diffusion of 10 mM $Fe(CpCO_2CH_3)_2$ in 1.5 M $LiClO_4$/MePEG-4000, 25 °C, $v = 0.1$ V/s, nearby Ag reference.

In a −11 °C glycerol solution, where diffusion is much slower, well-behaved linear diffusion voltammetry could be accessed, as illustrated by Figure 5B. The linear diffusion condition attained in a similar experiment, but at 1 °C, is illustrated in Figure 6 by the linearity of i_p vs $v^{1/2}$ (eq 2) obtained using the nearby Ag reference electrodes (Figure 6, ■) and the far-away (∼0.3 cm) Ag reference electrodes (Figure 6, ●). The latter are about 10% lower, presumably due to some ohmic distortion of the voltammogram. Figure 6, ▲, also shows voltammetric peak currents (on a 10-fold expanded current scale) obtained in the same

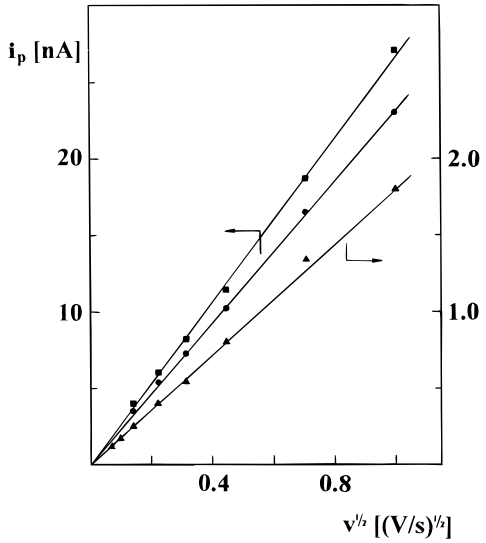

Figure 6. Plot of type D microband linear diffusion peak currents vs $v^{1/2}$ for cyclic voltammetry of 10 mM $CpFeCpCH_2CH_2OH$ in 0.1 M $LiClO_4$/glycerol at 1 °C at (▲) microdisk, $r = 23.8$ μm, slope $= 1.8 \times 10^{-9}$ A/s$^{1/2}$; (■) microband, $w = 2.7$ μm, $L = 0.7$ cm, $d = 3$ μm (nearby reference electrode), slope $= 2.64 \times 10^{-8}$ A/s$^{1/2}$; (●) same microband but far-away reference, $d = 0.3$ cm, slope $= 2.2 \times 10^{-8}$ A/s$^{1/2}$.

solution with a microdisk electrode of nominal surface area ∼10-fold smaller than the microband nominal area. Based on the slope of the i_p vs $v^{1/2}$ plot for the type D microband (with nearby reference electrode), the real area of this microband is ∼40% larger than its nominal value. Results from the voltammetry of Figure 5B, for a different microband sample, produced almost exact agreement between the microband and microdisk nominal areas (Table 1). Thus, type D electrodes can be (very nearly) quantitatively consistent with their planned geometries under linear diffusion conditions.

Type D microbands with nearby reference electrodes are designed for very slow diffusion and not for use in fluid solutions. The Ag strips are, after all, only pseudoreference electrodes that maintain a reasonably steady and reproducible potential only in the absence of species that strongly interact with the Ag surface or that supply a larger capacity redox equilibrium. In situations where the diffusion profile emanating from the microband encounters the nearby reference, its potential is disturbed and shifts, as illustrated by the fluid solution experiment in Figure 5C, where this has occurred. The hysteresis distorts the appearance of the ferrocene oxidation wave but, as expected, not the limiting current.

Type D microbands, while complex to assemble, have proven durable over a multiyear period when subjected only to light, infrequent polishing. Nonetheless, they eventually begin to exhibit real areas larger (10−20 fold) than nominal, suggesting gradual delamination of electrode microfoil from the adjoining insulator. Table 1 shows results[5] of testing two type "D-old" electrodes by chronoamperometrically measuring the diffusion coefficient for the Co(III/II) reaction in undiluted Co bipyridine redox polyether hybrid[2h,i] melts. These materials have large redox site concentrations and are extremely viscous, and the polyether-tailed metal complexes exhibit very slow self-diffusion rates (5×10^{-12} and 2×10^{-14} cm^2/s in the examples in Table 1, see footnotes *k* and *l*). Figure 7 shows area-normalized, chronoamperometric Cottrell plots obtained in a Co complex melt using one of the type D-old microbands (curves 1, 2, 3, and 6), a microdisk (curve 4),

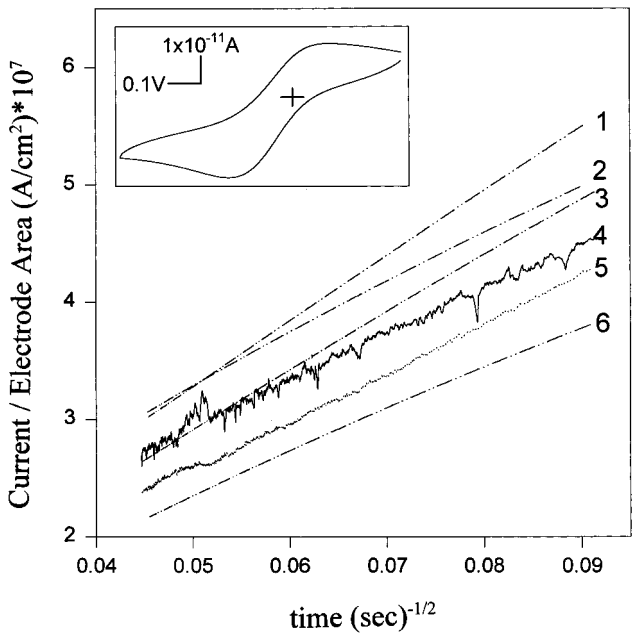

Figure 7. Area-normalized Cottrell plots for chronoamperometric potential steps ($120 < t < 500$ s) in a room temperature melt of [Co(bpy(CO_2PPPM)$_2$)$_3$](ClO_4)$_2$ (with 5% excess Co salt) on type D-old microband (1, 2, 3, 6) and on microdisk (4) and line (5) electrodes. Currents for microband Cottrell plots (1, 2, 3, 6) (Table 1, footnote *l*) were normalized on the basis of a "real" electrochemical area (12.6 times nominal), determined by comparison to (average of) Cottrell plots obtained with a 6.5 μm radius Pt microdisk (4) and a lithographically defined Pt line electrode (5). Inset shows typical quasi-reversible Co(III/II) cyclic voltammetry (scan rate = 0.2 mV/s; ΔE_{peak} = 201 mV) in the same melt using the microband electrode.

and a Pt line electrode (curve 5). Raw Cottrell plot slopes for the microbands that are based on nominal areas are larger than those of the microdisk and line electrodes; in Figure 7, the microband currents have been normalized using an excess (real) area factor of 12.6-fold. Comparable area factors for this electrode were also found using faster-diffusing melts, so the type D-old results in Figure 7 are not simply due to an exceptionally short diffusional path length.

Diffusion coefficients in the Co bipyridine redox polyether hybrid melts[2c,h,i,5] can be systematically manipulated ($\sim 10^{10}$ range) by variations in the character, number, length, and manner of attachment of the polyether chains and by addition of $LiClO_4$ electrolyte. Especially interesting are conditions that yield extremely small Co(III/II) diffusion coefficients ($\sim 10^{-18}$ cm^2/s has been recorded), since this gives access to "diffusion" path lengths of molecular dimensions[2c] and to measurements below glassing transitions, where transport data are classically a challenge.[24] Measurements of small diffusivities, when ionic conductivities are vanishingly small, are additionally important to our goal of developing methodology suitable for electroanalytical applications in solids and semisolids. In these circumstances, the favorable attributes of microbands, relative to microdisks, make knowledge of their real areas crucial.

Type C microbands were the widest tested in this work and were very well-behaved. Table 1 shows results for measurements under radial and linear diffusion conditions that show that these wide microbands behave ideally on both accounts. It seems that the wider the microband, the greater the ease in obtaining linear diffusion results that are in accord with the nominal electrode area. This is again consistent with the notion that the most usual kind of nonideality is a delamination from the insulator at the edges of the microband, the contribution of which is progressively a smaller part of the overall actual microband area, the greater the microband width.

Lithographically defined line microband electrodes should not suffer from delamination effects. Figure 7 shows a comparison of line (curve 5) and microdisk (curve 4) electrodes in a melt sample where the Co complex self-diffusion coefficient is rather small ($\sim 10^{-14}$ cm^2/s). The area-normalized Cottrell slopes in Figure 7 are in almost exact agreement (Table 1, line electrode). (Typically, however, measurements in the melts can vary by ~2-fold, which is a common level of uncertainty for very small diffusion coefficient determinations.) We conclude that the line and microdisk electrodes exhibit similar levels of ideality in real vs nominal surface area. The line electrodes, however, are capable of application to media with much smaller diffusion coefficients than are the microdisks; the area-normalized current axis in Figure 7 obscures the fact that the microdisk currents measured were 1 pA, while those measured with the line electrode were in the 0.1 nA range.

Theory for Uncompensated Resistance Effects under Linear Diffusion Conditions. As noted in the introduction, under linear diffusion conditions, microbands offer the advantage, relative to microdisks, of larger currents (mitigating small current measurement problems) yet retain good uncompensated solution resistance properties (iR_{UNC}). This property makes microbands attractive for measurements in which transport of the electroactive species and of the supporting electrolyte ions (i.e., large specific solution resistance, ρ) are both very slow. After presenting the relevant theory for iR_{UNC} effects at microdisks and at microbands, we will return to experiments exploring certain aspects of the theory.

Wightman and Wipf[3] have shown that the expression[25] for uncompensated resistance for a hemicylindrical working electrode of radius r_1 with a concentric hemicylindrical reference electrode of larger radius r_2,

$$R_{UNC} = \frac{\rho}{\pi L} \ln \frac{r_2}{r_2} \qquad (6)$$

can be adapted for a microband by equating the microband with a hemicyclinder of equivalent area (i.e., $w = \pi r_1 L$). Adopting the same relation for the reference hemicyclinder (i.e., $w + 2d = \pi r_2 L$, where d is the gap between microband and reference electrodes), eq 6 becomes

$$R_{UNC} = \frac{\rho}{\pi L} \ln\left[\frac{w + 2d}{w}\right] \qquad (7)$$

In cyclic voltammetry, the expression for the iR_{UNC} drop at a band electrode, under conditions of linear diffusion, is obtained from the product of eqs 2 and 7:

(24) (a) Inoue, T.; Cicerone, M. T.; Ediger, M. D. *Macromolecules* **1995**, *28*, 3425. (b) Blackburn, F. R.; Wang, C. Y.; Ediger, M. D. *J. Phys. Chem.* **1996**, *100*, 18249.

(25) Kasper, C. *Trans. Electrochem. Soc.* **1940**, *77*, 353.

$$iR_{UNC} = \frac{(2.69 \times 10^5) n^{3/2} \rho w v^{1/2} D^{1/2} C}{\pi} \ln\left[\frac{w + 2d}{w}\right] \quad (8)$$

This equation predicts that (a) at a microband, the uncompensated potential drop changes linearly with microband width, w, but (b) is *independent* of the length, L, so that (c) while increasing L increases linear diffusion current proportionately (eq 2), it does not increase the iR_{UNC} drop. Also, (d) when d approaches the microband width w (i.e., the reference electrode is placed very close to the microband, as in electrode type D), iR_{UNC} drop will become very small.

For microdisk electrodes, the uncompensated resistance expression[3,26]

$$R_{UNC} = \frac{\rho}{4\pi r}\left[1 - \frac{r}{d}\right] = \frac{\rho}{4\pi r} \quad (9)$$

collapses to the simpler equation shown when the reference−working electrode separation greatly exceeds the microdisk radius r (i.e., $d \gg r$). The product of eqs 2 and 9 shows that, under linear diffusion conditions, (a) at a microdisk the uncompensated potential drop changes linearly with microdisk radius, r, so that (b) changes in current caused by changes in r also change the iR_{UNC} drop.

Further insights into differences between microbands and microdisks, under linear diffusion conditions, come from the ratio of microband and microdisk currents (via eq 2),

$$\frac{i_{band}}{i_{disk}} = \frac{wL}{\pi r^2} \quad (10)$$

which shows, as seen already in the preceding section, that currents at microbands and microdisks with equivalent small dimensions (i.e., $w = r$) are much larger at the microband.

The relative values of uncompensated potential drops are obtained by combining eqs 7, 9, and 10:

$$\frac{iR_{UNC,band}}{iR_{UNC,disk}} = \frac{4w}{\pi r} \ln\left[\frac{w + 2d}{w}\right] \quad (11)$$

which leads to the important conclusion that the iR_{UNC} ratio for microbands and microdisks is determined mainly by the ratio of microband width to microdisk radius. The combination of eqs 10 and 11 further say that the (long axis-based) *enhancement of current at microbands comes about without concurrent enhancement of uncompensated resistance effects.* Perusal of the literature indicates that, while this conclusion may be appreciated, it has not been outlined in detail nor experimentally verified.

Results for Resistance Effects at Microbands and Microdisks. The uncompensated resistance-based potential drops at microbands and microdisks were evaluated using the cyclic voltammetry of a reversible (ferrocene) redox couple under linear diffusion conditions. For sufficiently small resistance effects, iR_{UNC} is expected to enlarge the potential peak separation over the reversible value by an amount that depends on the potential sweep rate; the total is

(26) Newman, J. *J. Electrochem. Soc.* **1966**, *113*, 501.

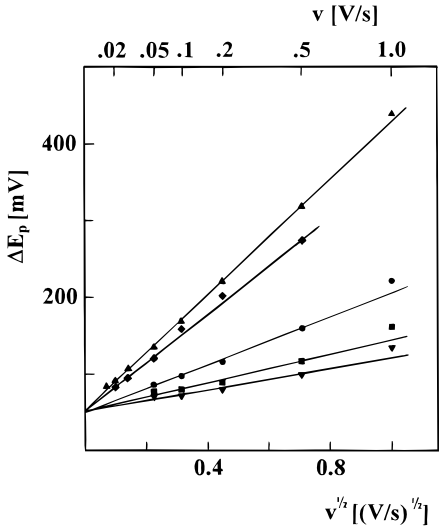

Figure 8. Plots of ΔE_{peak} vs $v^{1/2}$ where v is the potential sweep rate, for linear diffusion cyclic voltammetry experiments in 10 mM $CpFeCpCH_2CH_2OH$ in $LiClO_4$/glycerol: (▼, ■) microband, 0.1 M $LiClO_4$, 1 °C, w = 2.7 μm, L = 0.7 cm, d = 3 μm (nearby Ag reference); (●) same microband but far-away reference, d = 0.3 cm, 0.1 M $LiClO_4$ at 1 °C; (◆) same microband but nearby Ag reference, 0.1 M $LiClO_4$, −20 °C; (▲) microdisk, 0.1 M $LiClO_4$, 1 °C, r = 23.8 μm.

Table 2. Results for Uncompensated Resistances under Linear Diffusion at Type D Microbands and at Microdisks

electrode	ref	T, °C	$LiClO_4$, M	ΔE_{peak} vs $v^{1/2}$ slope	ΔE_{peak} vs $v^{1/2}$ intercept	R_{UNC}, MΩ
band[a]	nearby	+1[d]	0.1	0.085[f]	55[g]	1.6
band[a]	far-away	+1	0.1	0.155[f]	49[g]	2.8
band[a]	nearby	+1	1.0	0.069[f]	51[g]	1.3
band[a]	nearby	−20[e]	0.1	0.314	52[h]	41
disk, r = 24 μm[b]	far-away	+1	0.1	0.370	53[g]	101
disk, r = 52 μm[c]	nearby	+1	0.1	0.367	61[g]	19

[a] Area = 1.9×10^{-4} cm^2. [b] Area = 1.8×10^{-5} cm^2. [c] Area = 8.5×10^{-5} cm^2. [d] $D = 1.3 \times 10^{-9}$ cm^2/s. [e] $D = 4.8 \times 10^{-11}$ cm^2/s. [f] For first four points, Figure 8. [g] $2.3RT/F$ = 54 mV. [h] $2.3RT/F$ = 50 mV.

$$\Delta E_{peak} = \frac{2.3RT}{nF} + 2i_p R_{UNC} \quad (12)$$

Since linear diffusion current (i_p) varies linearly with $v^{1/2}$, a plot of ΔE_{peak} vs $v^{1/2}$ should be linear, with an intercept equal to the reversible ΔE_{peak} and a slope from which the uncompensated resistance can be obtained for comparison to eqs 7 and 9.

ΔE_{peak} results from the microdisk (▲) and type D microband (▼, ●) experiments of Figure 6 (which demonstrated linear diffusion) are shown in Figure 8 (▼, ●, ▲), along with two other experiments. In accord with eq 12, the plots are nearly linear at lower scan rates; the positive deviations in ΔE_{peak} at scan rates higher than 0.5 V/s are probably due to the concurrent distortions of the voltammetric wave shapes and of the $i_p/v^{1/2}$ relation there. The intercepts, slopes, and values of R_{UNC} calculated from the slopes are given in Table 2. The intercepts are uniformly close to the theoretical values at the corresponding temperatures. Table 2 also shows results from other experiments in which a higher electrolyte concentration (a lowered R_{UNC} results) and a lower temperature (a larger R_{UNC} results) are employed.

The Table 2 results at 1 °C show that the magnitude of R_{UNC} strongly reflects the microelectrode design. Thus, R_{UNC} at the

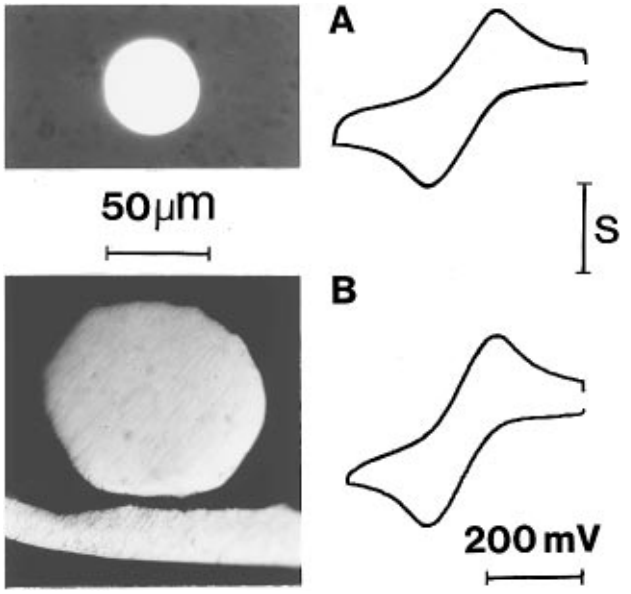

Figure 9. Optical micrographs of two microdisk electrodes and cyclic voltammograms obtained at 50 mV/s with them in a 10 mM $CpFeCpCH_2CH_2OH$ in glycerol/0.1 M $LiClO_4$ at 1 °C; (A) radius = 23.8 μm, S = 0.4 nA; (B) radius = 53 μm, S = 2 nA.

microdisk is considerably larger than that at the microbands, and R_{UNC} at the microband is less when using a nearby vs a far-away reference electrode. Comparing the results to theory, the ratio of microband to microdisk experimental R_{UNC} values is 0.016 and 0.028 for nearby and far-away microband reference electrodes, respectively, whereas the predicted ratios (from eqs 7 and 9) are 0.005 and 0.033, respectively. The agreement with theory ranges from exact to ~3-fold. The ratio of experimental R_{UNC} values found using the microband with nearby vs far-away reference is 0.15; the ratio predicted using eq 7 (the ratio of the "ln" terms written for differing d values) is 0.57, a 3.8-fold difference. It would appear from these two comparisons that the experimental resistance of the microband with nearby reference electrode, while definitely decreased, remains about 3−4-fold larger than the theory predicts.

The effect of a nearby reference electrode was also evaluated for a microdisk fabricated as described in the Experimental Section; a micrograph is shown in Figure 9. In this case, the disk/reference separation is only about 5 μm, which is less than the microdisk radius (52 μm), i.e., $d < r$. Equation 9 is meaningless under this circumstance. Table 2 (disk, nearby) shows that, while the uncompensated resistance remains substantial for this electrode, it is nonetheless reduced by about 5-fold relative to the 24 μm radius microdisk. Conventional wisdom[3] is that the effective solution resistance is inversely proportional to the smallest electrode dimension. In the present case, it is the nearby reference electrode which is responsible for the reduced resistance at the larger microdisk. The microdisk with nearby reference in Figure 9 is relatively easy to fabricate and, due to the side-by-side placement of working and reference electrodes, avoids current shielding effects.[11]

CONCLUSIONS

First, testing microbands under conditions of linear diffusion is a methodology that reveals the real microband area and can point to defects such as electrode/insulator delamination that are not indicated by experiments under radial diffusion conditions. Linear diffusion real-area evaluation of microbands, or some equivalent real-area approach (such as electrode capacitance, heterogeneous electron transfer rate constant, or underpotential monolayer deposition), is essential for their full characterization and, indeed, for any miniaturized electrode design. Very thin, sandwich-type microbands should be especially suspect in this regard.

Second, under identical linear diffusion experimental conditions, microband electrodes exhibit considerably larger currents as compared to those of microdisks with comparable smallest dimension, while at the same time displaying iR_{UNC} values that are similar to those of microdisks. These seemingly contradictory attributes are predicted by theory and are consistent with experimental results. Provided that the real microband area is known, or is determined, microbands are powerful tools for study of viscous, ionically resistive media at longer time scales.

Finally, microband and microdisk electrodes can be designed so as to have reference electrodes as close as the same dimension of the microelectrode itself. Under linear diffusion conditions where the diffusion layer depth is even smaller, this close proximity of reference and working electrodes can significantly reduce uncompensated resistance effects.

ACKNOWLEDGMENT

The authors thank Mr. Zohar Barkai (NRC-Negev) for assistance with SEM measurements and Dr. C. Velazquez for part of Figure 5. This research was supported in part by grants from the National Science Foundation and the Office of Naval Research.

SUPPORTING INFORMATION AVAILABLE

Photograph and detailed fabrication procedures for type A, B, and D microbands (5 pages). Ordering information is given on any current masthead page.

Received for review July 24, 1997. Accepted October 2, 1997.[⊗]

AC970803D

[⊗] Abstract published in *Advance ACS Abstracts,* November 15, 1997.